Letter

Ferroic dislocations in paraelectric $SrTiO_3$

Takahiro Shimada,[1,*] Kairi Masuda,[1,†] Youhei Hagiwara,[1] Naoki Ozaki,[1] Tao Xu,[2] Jie Wang,[3] and Takayuki Kitamura[1]

[1]*Department of Mechanical Engineering and Science, Kyoto University, Nishikyo-ku, Kyoto 615-8540, Japan*

[2]*Ningbo Institute of Materials Technology and Engineering, Chinese Academy of Sciences, Ningbo 315201, China*

[3]*Department of Engineering Mechanics, School of Aeronautics and Astronautics, Zhejiang University, Hangzhou 310027, China*

(Received 17 August 2020; revised 19 January 2021; accepted 21 January 2021; published 3 February 2021)

Ferroic systems under considerable geometrical restrictions at nanoscale have successfully introduced novel phases such as multiferroic and topological phases. However, ferroic orders completely disappear below the critical size limit of several nanometers and the geometry cannot be relied upon to produce a variety of phases. Here, via first-principles calculations, we demonstrate that a rich variety of phases and their transitions can be realized by dislocations in paraelectric $SrTiO_3$. We show that atomic-scale ferroelectricity and (anti)ferromagnetism are induced by the strain concentration and nonstoichiometry intrinsic to dislocations in $SrTiO_3$, resulting in ferroelectric-(anti)ferromagnetic-multiferroic phase transitions depending on the core structure. Furthermore, we also show that electrical polarization configurations strongly depend on the strain distribution around a dislocation and topological phases can be realized without geometrical restrictions. The present result suggests that the utilization of defects in a material is a powerful strategy to design ferroic orders below the critical size, thereby expanding the application of ferroic nanostructures to the atomic scale.

DOI: 10.1103/PhysRevB.103.L060101

Ferroic phases and associated transitions have been subjects of intensive research due to their fascinating physical properties. In particular, integrating multiferroic phases [1–4] in which ferroelectric and ferromagnetic orders coexist and interact, has been one of the goals in materials science today because their electromagnetic coupling stimulates technological innovations [5–8]. However, despite the extensive quest for new multiferroics, few materials exhibit multiferroic phases because of the mutually exclusive mechanism of ferroelectricity and ferromagnetism [9]. That is, an empty d orbital drives ferroelectricity while a partially filled d state is required for magnetism. To overcome this mechanism, researchers have focused on the surface or interfacial geometries of materials. In multiferroic composites that are composed of ferroelectric and ferromagnetic materials, these orders are coupled through deformation at the interface [10–12], and even reversal of the magnetization by electric fields has been achieved [13]. In addition, our knowledge of phase transitions has been expanded by intense surface and interface effects at nanoscale. Magnetism by excess electrons at the surfaces of the ferroelectric nanostructures induces unusual size-dependent ferroelectric-multiferroic-(anti)ferromagnetic phase transitions [14]. Moreover, the strong depolarization fields at nanoscale generate unconventional topological phases [15–17] such as polarization vortices in ferroelectric nanodots [18,19], producing a new class of multiferroics with ferroelectricity and ferrotoroidicity [20–22]. Thus, the design of phase transitions by material geometry has been undoubtedly successful. However, in the surging demand for miniaturization to increase the speed and capacity of integrated devices such as memories, it has been demonstrated that the depolarization fields in nanoscale materials also destabilize ferroic orders below the critical size [23–25], which is 3–5 nm in ferroelectric nanodots [26]. Therefore, the additional miniaturization of certain devices while retaining desirable properties is physically challenging, also indicating that the material geometry is no longer reliable to induce novel phase transitions at such an extremely small scale. Thus, an alternative strategy is needed for further scale down and design of ferroic materials.

Dislocations, which are one-dimensional lattice defects, are pervasive in materials and typically detrimental to material properties and device functionality due to atomic disorder [27–29]. However, these defects act as one-dimensional functional elements in some cases because of the atomic-scale mechanical and chemical properties [30–32]. As an example, it is experimentally demonstrated that dislocations in insulating ceramics exhibit conductivity since the elastic field and nonstoichiometry limited to a few lattices around dislocations locally alter electronic properties, indicating that this defect is an atomic-scale conductive channel embedded in the material [33,34]. According to the progress in the ability to manipulate dislocations in materials, a recent emerging concept of dislocation engineering has expanded our knowledge of material design, suggesting the possibility of fabricating extremely thin ferroic phases and their transitions at the atomic scale.

Here, we demonstrate a rich variety of ferroic orders under the critical size limit and their transitions can be realized by dislocations in paraelectric $SrTiO_3$. The first-principles calculations reveal that the strain concentration

*shimada@me.kyoto-u.ac.jp

†masuda.kairi.64n@st.kyoto-u.ac.jp

caused by dislocations induces electrical polarization limited to a few lattices while the nonstoichiometry of the atomic disorder brings highly localized spin moments, resulting in the atomic-scale ferroelectric-(anti)ferromagnetic-multiferroic phase transitions depending on the core structure. Furthermore, we also show that the strong dependence of the polarization configurations on the strain fields of dislocations may generate atomic-scale topological phases. Our results indicate a new strategy for the realization of a rich variety of ferroic orders below the critical size limit, thereby expanding the application of ferroic nanostructures into the atomic scale.

Single $SrTiO_3$ edge dislocations were simulated from first-principles calculations within the density functional theory using the VASP code [35–38]. The exchange-correlation energy was treated by employing the generalized gradient approximation [39] corrected with the Perdew-Burke-Ernzerhof revised for solids (PBEsol) [40]. Furthermore, to evaluate localized electrons accurately, the energy was also corrected with an on-site Hubbard correction U [41], applying values of $U = 4.96$ eV and $J = 0.51$ eV, respectively [42]. The dislocations were studied via the periodic supercell approach using the dipole model [43], as shown in Supplemental Material Fig. S1. Since core-core interactions are canceled out in the dipole model, single dislocations can be investigated even under periodic conditions. The dislocation distances were set to greater than 20 Å with the dimensions of the supercell along the three cell vectors being 11a, 7a, and 2a, respectively. We carefully checked that interactions between dislocations, including elastic and electric interactions, are negligible by this model size. Here, since the core region is no longer a simple unit cell, vacancies are formed to stabilize a dislocation. Both the Ti-rich dislocation with O vacancies (V_O) and the Sr-rich dislocation with Sr vacancies (V_{Sr}) were considered by removing O and Sr atoms, which are electrically neutral, based on experimental observations and theoretical implications [44–46]. The stabilities of these core structures have further been validated by calculating the formation energy (Supplemental Material Table S1). Full details of the computational methods are available in the Supplemental Material [47]). Moreover, the $SrTiO_3$ screw dislocations were simulated in the same way as the edge dislocations via the periodic supercell approach as shown in Fig. S2. The dislocation distances were set to 20 Å, with the dimensions of the supercell along the three cell vectors being 10a, 7a, and 2a, respectively. O deficiencies were introduced based on experimental observations [48,49]. The stabilities of the core structure have further been validated by calculating the formation energy (Supplemental Material Table S2).

The ferroelectric properties of the edge dislocations were investigated by introducing a site-by-site local polarization based on atomic displacements and the Born effective charges [47,50]. The polarization distribution of the Sr-rich dislocation shows that the polarization vectors point in the x direction localized to a few lattices right under the core, with the maximum polarization being $1.36\,C/m^2$ [Fig. 1(a1)]. This has a long-range order along with the dislocation and thus can be regarded as ferroelectricity. The emergence of this localized ferroelectricity is attributed to the tensile strain concentration under the edge dislocation (Supplemental Material Fig. S3) because $SrTiO_3$ undergoes the paraelectric-ferroelectric phase transitions under tension [51–54]. This polarization should

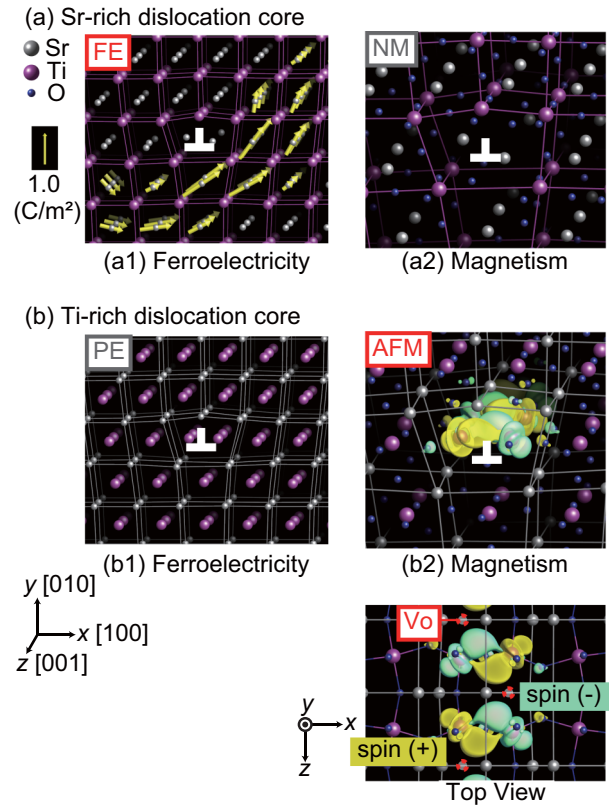

FIG. 1. Polarization and magnetic spin density distributions of (a) Sr-rich and (b) Ti-rich edge dislocations in $SrTiO_3$. In the polarization distribution, oxygen atoms are not shown for clarity and the yellow arrows indicate polarization vectors. In the magnetic distributions, the yellow and green areas indicate the isosurfaces of spin densities of $+0.03$ and -0.03 $\mu_B/Å^3$, respectively.

be switched by external electric fields as well as usual ferroelectrics since polarization pointing in the right direction [Fig. 1(a1)] and the left direction [inversion of Fig. 1(a1)] is equivalent to the dislocation. On the other hand, the Ti-rich dislocation exhibits no polarization [Fig. 1(b1)], indicating the involvement of other mechanisms in the emergence of ferroelectricity. Moreover, the Ti-rich dislocation in the intrinsically nonmagnetic $SrTiO_3$ exhibits magnetic moments of $0.51\mu_B$ that are localized at the Ti atoms of dislocation core in an antiferromagnetic (AFM) configuration [Fig. 1(b2)], while no moment is observed in the Sr-rich dislocation [Fig. 1(a2)]. This emerging magnetism also cannot be attributed to the elastic field of the edge dislocations.

To elucidate the underlying mechanism for the emergence of the ferroelectricity and (anti)ferromagnetism, the electronic band structures were analyzed. Four distinct electronic states are observed within the band gap (lower states) and the conduction band (upper states) of the Ti-rich dislocation core as shown in Fig. 2(a). Both states are occupied by majority-spin and minority-spin electrons, whereas the upper degenerate states possess metallic characteristics. These four states are absent in a perfect $SrTiO_3$ crystal and are therefore characteristic of defect states that are introduced by the dislocation structure. These spin-polarized excess electrons originate from the nonstoichiometry of the dislocation core.

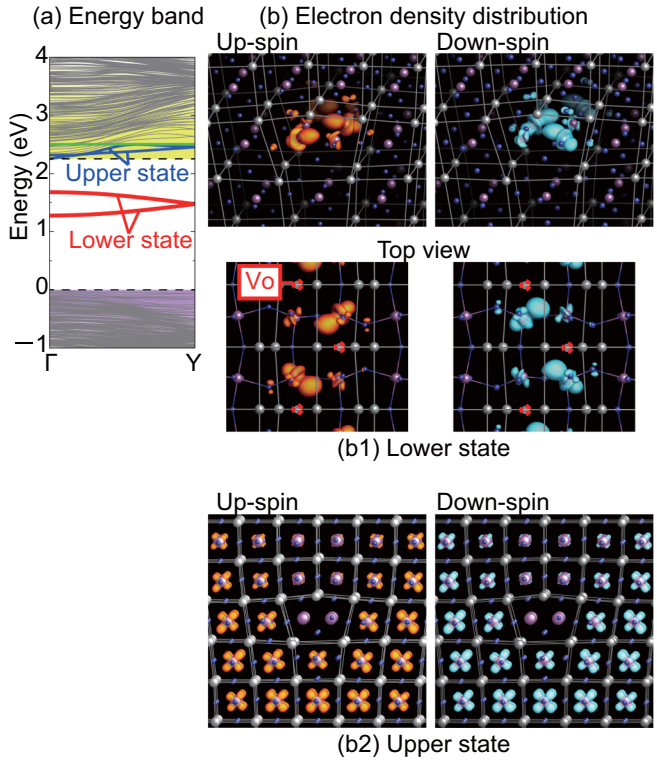

FIG. 2. (a) Electronic band structure of Ti-rich dislocations. The green line indicates the Fermi level. The blue and red lines indicate the upper state band and lower state band, respectively. (b1) Localized electron density distributions of the lower state band. The orange and light-blue isosurfaces represent the up-spin and down-spin densities of 0.03 $Å^{-3}$. (b2) Electron density distributions of the upper state. The orange and light-blue isosurfaces represent the up-spin and down-spin densities of 0.001 $Å^{-3}$.

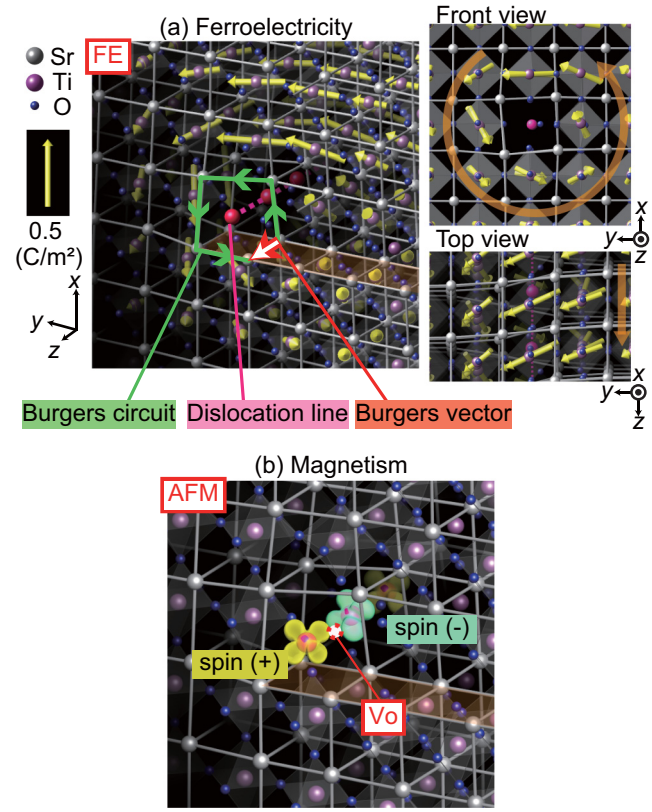

FIG. 3. (a) Polarization and (b) magnetic spin density distributions of screw dislocations in $SrTiO_3$. In the polarization distribution, the yellow arrows indicate polarization vectors. In the magnetic distribution, the yellow and green areas indicate the isosurfaces of spin densities of $+0.03$ and -0.03 $\mu_B/Å^3$, respectively.

The atomic composition of the Ti-rich dislocation system is composed of 110 Sr, 112 Ti, and 326 O atoms, which deviates from the stoichiometric composition 1:1:3 of bulk $SrTiO_3$. This nonstoichiometric composition results in a net charge of $+8$ per dislocation based on the nominal ionic charges of Sr^{2+}, Ti^{4+}, and O^{2-}. The shape of the squared wave functions indicates that the lower states that accommodate the majority and minority spin electrons are ascribed to the *d*-dominant orbitals that are separately localized at the Ti atoms [Fig. 2(b1) and Supplemental Material Fig. S4). These localized and separated spin-polarized electrons induce the antiferromagnetism around the core center. On the other hand, ferroelectricity is suppressed by free carriers accommodated in the upper states [Fig. 2(b2)] since these delocalized electrons screen electrostatic interactions that are responsible for electronic polarization. Thus, the Ti-rich dislocation exhibits magnetism but not ferroelectricity. Here, dilute magnetism at grain boundaries of nonmagnetic materials, which is likely to derive from the same mechanism as this study, is measured even at room temperature, indicating that magnetism around the dislocation can be utilized for device applications [55]. In the case of the Sr-rich dislocation, however, the whole valence state that is determined to be 0 with the composition of 108 Sr, 110 Ti, and 328 O atoms inhibits the spin polarization and screening, resulting in nonmagnetic but ferroelectricity. Thus, we conclude that electrical polarization and spin moments do not coexist around the edge dislocations.

In contrast, the ferroelectricity and magnetism effectively coexist around the screw dislocation. The local polarization comprises a mixture of the nonzero axial polarization components and a vortex pattern, i.e., spiral polarization [Fig. 3(a)] that is localized to a few lattices with the maximum polarization being 0.62 C/m^2 (Supplemental Material Fig. S5). The shear strain concentration around the screw dislocation (Supplemental Material Fig. S6) is responsible for the emergence of this localized spiral pattern. Surprisingly, an antiferromagnetic spin configuration with local magnetic moments of $0.80\mu_B$ is formed at the core region despite the mutual exclusive mechanism of ferroelectricity and ferromagnetism, resulting in multiferroicity at the atomic scale. We shed light on the mechanism of the multiferroicity around the screw dislocation from electronic-level insights. The screw dislocation is composed of 100 Sr, 100 Ti, and 298 O atoms that results in a net charge of $+2$ per dislocation. These excess electrons induce the formation of a new state accommodating the majority and minority spins within the band gap as shown in Fig. 4(a). As in the Ti-rich edge dislocation, the antiferromagnetic ordering is ascribed to this new state in which *d*-dominant orbitals are separately localized at the two Ti atoms [Fig. 4(b) and Supplemental Material Fig. S7). Unlike in the edge dislocation, however, there are no excess electrons

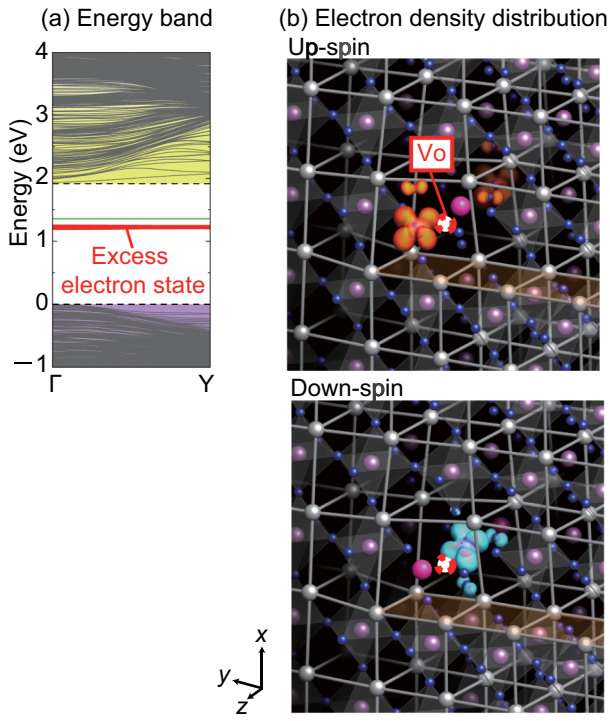

FIG. 4. (a) Electronic band structures of screw dislocations. The green line indicates the Fermi level. The red line indicates an excess electron state. (b) Localized electron density distributions at the excess electron state. The orange and light-blue isosurfaces represent the up-spin and down-spin densities of 0.03 Å, respectively.

that screen the electronic polarization. These result in the coexistence of ferroelectricity and (anti)ferromagnetism around the screw dislocation.

Depending on the core structure, the dislocations undergo ferroelectric-(anti)ferromagnetic-multiferroic phase transitions that are localized to a few lattices around the core. These localized emerging ferroic properties are embedded within the ambient paraelectric host and enable the dislocation structure to act as an atomic-scale ferroelectric-(anti)ferromagnetic-multiferroic channel below the critical size. Moreover, the tensile strain around the edge dislocation generates a rectilinear polarization configuration while the shear strain around the screw dislocation induces a spiral configuration that is accompanied by ferrotoroidicity. Since a state with unusual symmetry breaking such as chirality by vortices is called a topological phase, this indicates that the nontopological-topological phase transitions, which have so far been driven by geometrical restrictions, occur at the atomic scale due to the variation in the dislocation core structures. Here, although our targets in this study are simple dislocations with electrically neutral vacancies, they can be more complicated such as mixed dislocations or charged depending on external conditions, which may bring more various polarization configurations. Therefore, a rich variety of phases, including multiferroic and topological phases, can be realized even below the critical size limit and their transitions are tuned by dislocation structures in $SrTiO_3$. These results cannot be achieved by conventional strategies using geometrical constraints and have significant technological implications. As an example, a dislocation with ferroelectric orders may be utilized as a memory bit. Since dislocations with a sufficiently high density (up to 10^{12} cm^{-2}) have been intentionally introduced in experiments [30], the vast data density of Pbit/in^2 can be realized by dislocations, clearly beyond the several Tbit/in^2 limited by the critical ferroelectric size of 3–5 nm. Furthermore, the additional degrees of freedom, i.e., ferromagnetic and ferrotoroidicity, permit us to increase the number of states of dislocation and tune the response to the external fields at the atomic scale, suggesting that the above ultrahigh data density can be further increased and manipulated by various fields.

On the other hand, our study indicates at the same time that defects play a predominant role when ferroics reduce to atomic-scale in size. This leads to engineering ferroics based on intriguing properties of defects, which will surely further expand the potential application. In other words, the same as bulk and nanoferroics are different due to surface effects, nano- and atomic ferroics may be different due to defects. For example, polarization configurations can be engineered by interactions with other vacancies and dislocations, which may be impossible for larger ferroics. Moreover, different from ordinal dislocations which hold inversion symmetry, ferroic dislocations can represent 1 and 0 depending on the direction of polarization. On the other hand, dislocations move by external mechanical loads. These indicate that ferroic dislocations function as information careers driven by mechanical loads, suggesting a mechanically controlled circuit that can harvest environmental vibration and thus is energy saving.

In summary, we have proposed a design strategy for atomic-scale ferroics through the engineering of otherwise detrimental dislocations in paraelectric $SrTiO_3$. Our theoretical predictions revealed that the strain concentration and nonstoichiometry of the dislocations induce ferroelectricity and (anti)ferromagnetism which are localized to a few lattices around the core. These result in a ferroelectric Sr-rich edge dislocation, a magnetic Ti-rich edge dislocation, and a multiferroic screw dislocation. These dislocations are atomically fine ferroic channels below the critical size encompassed by the peripheral paraelectric host. Moreover, we have also demonstrated that electrical polarization configurations are strongly dependent on the strain distribution around the dislocations. This creates a rectilinear configuration around the edge dislocation while a spiral configuration around the screw dislocation. Therefore, the dislocations undergo ferroelectric-(anti)ferromagnetic-multiferroic phase transitions and nontopological-topological phase transitions at the atomic scale based on the core structure. Thus, a rich variety of ferroic phases exist even below the critical size limit and they may be tuned by dislocation cores, extending applications of ferroic structures into an extremely small scale.

This work was supported by JSPS KAKENHI Grants No. JP18H05241, No. JP18H03753, and No. JP18K18807.

[1] J. Wang, J. B. Neaton, H. Zheng, V. Nagarajan, S. B. Ogale, B. Liu, D. Viehland, V. Vaithyanathan, D. G. Schlom, U. V. Waghmare *et al.*, Epitaxial $BiFeO_3$ multiferroic thin film heterostructures, Science **299**, 1719 (2003).

[2] M. Fiebig, T. Lottermoser, D. Fröhlich, A. V. Goltsev, and R. V. Pisarev, Observation of coupled magnetic and electric domains, Nature (London) **419**, 818 (2002).

[3] T. Kimura, T. Goto, H. Shintani, K. Ishizaka, T. Arima, and Y. Tokura, Magnetic control of ferroelectric polarization, Nature (London) **426**, 55 (2003).

[4] D. M. Juraschek, M. Fechner, A. V. Balatsky, and N. A. Spaldin, Dynamical multiferroicity, Phys. Rev. Mater. **1**, 014401 (2017).

[5] N. A. Spaldin and R. Ramesh, Advances in magnetoelectric multiferroics, Nat. Mater. **18**, 203 (2019).

[6] W. Eerenstein, N. D. Mathur, and J. F. Scott, Multiferroic and magnetoelectric materials, Nature (London) **442**, 759 (2006).

[7] S. Manipatruni, D. E. Nikonov, and I. A. Young, Beyond CMOS computing with spin and polarization, Nat. Phys. **14**, 338 (2018).

[8] S. Manipatruni, D. E. Nikonov, C. C. Lin, T. A. Gosavi, H. Liu, B. Prasad, Y. L. Huang, E. Bonturim, R. Ramesh, and I. A. Young, Scalable energy-efficient magnetoelectric spin-orbit logic, Nature (London) **565**, 35 (2019).

[9] N. A. Hill, Why are there so few magnetic ferroelectrics? J. Phys. Chem. B **104**, 6694 (2000).

[10] C. W. Nan, M. I. Bichurin, S. Dong, D. Viehland, and G. Srinivasan, Multiferroic magnetoelectric composites: Historical perspective, status, and future directions, J. Appl. Phys. **103**, 031101 (2008).

[11] R. Cai, V. A. Antohe, Z. Hu, B. Nysten, L. Piraux, and A. M. Jonas, Multiferroic nanopatterned hybrid material with room-temperature magnetic switching of the electric polarization, Adv. Mater. **29**, 1604604 (2017).

[12] H. Zheng, J. Wang, S. E. Lofland, Z. Ma, L. Mohaddes-Ardabili, T. Zhao, L. Salamanca-Riba, S. R. Shinde, S. B. Ogale, F. Bai *et al.*, Multiferroic $BaTiO_3$-$CoFe_2O_4$ nanostructures, Science **303**, 661 (2004).

[13] J. A. Mundy, C. M. Brooks, M. E. Holtz, J. A. Moyer, H. Das, A. F. Rébola, J. T. Heron, J. D. Clarkson, S. M. Disseler, Z. Liu *et al.*, Atomically engineered ferroic layers yield a room-temperature magnetoelectric multiferroic, Nature (London) **537**, 523 (2016).

[14] T. Shimada, T. Xu, Y. Uratani, J. Wang, and T. Kitamura, Unusual multiferroic phase transitions in $PbTiO_3$ nanowires, Nano Lett. **16**, 6774 (2016).

[15] Y. Nahas, S. Prokhorenko, L. Louis, Z. Gui, I. Kornev, and L. Bellaiche, Discovery of stable skyrmionic state in ferroelectric nanocomposites, Nat. Commun. **6**, 8542 (2015).

[16] S. Das, Y. L. Tang, Z. Hong, M. A. P. Gonçalves, M. R. McCarter, C. Klewe, K. X. Nguyen, F. Gómez-Ortiz, P. Shafer, E. Arenholz *et al.*, Observation of room-temperature polar skyrmions, Nature (London) **568**, 368 (2019).

[17] A. K. Yadav, C. T. Nelson, S. L. Hsu, Z. Hong, J. D. Clarkson, C. M. Schlepütz, A. R. Damodaran, P. Shafer, E. Arenholz, L. R. Dedon *et al.*, Observation of polar vortices in oxide superlattices, Nature (London) **530**, 198 (2016).

[18] I. I. Naumov, L. Bellaiche, and H. Fu, Unusual phase transitions in ferroelectric nanodisks and nanorods, Nature (London) **432**, 737 (2004).

[19] J. Wang, Switching mechanism of polarization vortex in single-crystal ferroelectric nanodots, Appl. Phys. Lett. **97**, 192901 (2010).

[20] N. A. Spaldin, M. Fiebig, and M. Mostovoy, The toroidal moment in condensed-matter physics and its relation to the magnetoelectric effect, J. Phys.: Condens. Matter **20**, 434203 (2008).

[21] T. Shimada, L. V. Lich, K. Nagano, J. Wang, and T. Kitamura, Hierarchical ferroelectric and ferrotoroidic polarizations coexistent in nano-metamaterials, Sci. Rep. **5**, 14653 (2015).

[22] S. Prosandeev, I. Ponomareva, I. Kornev, and L. Bellaiche, Control of Vortices by Homogeneous Fields in Asymmetric Ferroelectric and Ferromagnetic Rings, Phys. Rev. Lett. **100**, 047201 (2008).

[23] J. Junquera and P. Ghosez, Critical thickness for ferroelectricity in perovskite ultrathin films, Nature (London) **422**, 506 (2003).

[24] D. D. Fong, G. B. Stephenson, S. K. Streiffer, J. A. Eastman, O. Auciello, P. H. Fuoss, and C. Thompson, Ferroelectricity in ultrathin perovskite films, Science **304**, 1650 (2004).

[25] L. Despont, C. Koitzsch, F. Clerc, M. G. Garnier, P. Aebi, C. Lichtensteiger, J. M. Triscone, F. J. Garcia de Abajo, E. Bousquet, and P. Ghosez, Direct evidence for ferroelectric polar distortion in ultrathin lead titanate perovskite films, Phys. Rev. B **73**, 094110 (2006).

[26] M. J. Polking, M. G. Han, A. Yourdkhani, V. Petkov, C. F. Kisielowski, V. V. Volkov, Y. Zhu, G. Caruntu, A. P. Alivisatos, and R. Ramesh, Ferroelectric order in individual nanometre-scale crystals, Nat. Mater. **11**, 700 (2012).

[27] A. Lubk, M. D. Rossell, J. Seidel, Y. H. Chu, R. Ramesh, M. J. Hÿtch, and E. Snoeck, Electromechanical coupling among edge dislocations, domain walls, and nanodomains in $BiFeO_3$ revealed by unit-cell-wise strain and polarization maps, Nano Lett. **13**, 1410 (2013).

[28] M. J. Hÿtch, J. L. Putaux, and J. M. Pénisson, Measurement of the displacement field of dislocations to 0.03 Å by electron microscopy, Nature (London) **423**, 270 (2003).

[29] S. P. Alpay, I. B. Misirlioglu, V. Nagarajan, and R. Ramesh, Can interface dislocations degrade ferroelectric properties? Appl. Phys. Lett. **85**, 2044 (2004).

[30] I. Sugiyama, N. Shibata, Z. Wang, S. Kobayashi, T. Yamamoto, and Y. Ikuhara, Ferromagnetic dislocations in antiferromagnetic NiO, Nat. Nanotechnol. **8**, 266 (2013).

[31] T. Shimada, T. Xu, Y. Araki, J. Wang, and T. Kitamura, Multiferroic dislocations in ferroelectric $PbTiO_3$, Nano Lett. **17**, 2674 (2017).

[32] K. Szot, W. Speier, G. Bihlmayer, and R. Waser, Switching the electrical resistance of individual dislocations in single-crystalline $SrTiO_3$, Nat. Mater. **5**, 312 (2006).

[33] A. Nakamura, K. Matsunaga, J. Tohma, T. Yamamoto, and Y. Ikuhara, Conducting nanowires in insulating ceramics, Nat. Mater. **2**, 453 (2003).

[34] Y. Tokumoto, S. Amma, N. Shibata, T. Mizoguchi, K. Edagawa, T. Yamamoto, and Y. Ikuhara, Fabrication of electrically conductive nanowires using high-density dislocations in AlN thin films, J. Appl. Phys. **106**, 124307 (2009).

[35] G. Kresse and J. Hafner, *Ab initio* molecular dynamics for liquid metals, Phys. Rev. B **47**, 558 (1993).

[36] G. Kresse and J. Furthmüller, Efficient iterative schemes for *ab initio* total-energy calculations using a plane-wave basis set, Phys. Rev. B **54**, 11169 (1996).

[37] P. E. Blöchl, Projector augmented-wave method, Phys. Rev. B **50**, 17953 (1994).

[38] H. J. Monkhorst and J. D. Pack, Special points for Brillouin-zone integrations, Phys. Rev. B **13**, 5188 (1976).

[39] J. P. Perdew, K. Burke, and M. Ernzerhof, Generalized Gradient Approximation Made Simple, Phys. Rev. Lett. **77**, 3865 (1996).

[40] J. P. Perdew, A. Ruzsinszky, G. I. Csonka, O. A. Vydrov, G. E. Scuseria, L. A. Constantin, X. Zhou, and K. Burke, Restoring the Density-Gradient Expansion for Exchange in Solids and Surfaces, Phys. Rev. Lett. **100**, 136406 (2008).

[41] V. I. Anisimov, J. Zaanen, and O. K. Andersen, Band theory and Mott insulators: Hubbard U instead of Stoner I, Phys. Rev. B **44**, 943 (1991).

[42] X. Hao, Z. Wang, M. Schmid, U. Diebold, and C. Franchini, Coexistence of trapped and free excess electrons in $SrTiO_3$, Phys. Rev. B **91**, 085204 (2015).

[43] S. K. Yadav, R. Ramprasad, A. Misra, and X. Y. Liu, Core structure and Peierls stress of edge and screw dislocations in TiN: A density functional theory study, Acta Mater. **74**, 268 (2014).

[44] Z. Zhang, W. Sigle, and M. Rühle, Atomic and electronic characterization of the a[100] dislocation core in $SrTiO_3$, Phys. Rev. B **66**, 094108 (2002).

[45] S. Y. Choi, J. P. Buban, M. Nishi, H. Kageyama, N. Shibata, T. Yamamoto, S. J. L. Kang, and Y. Ikuhara, Dislocation structures of low-angle boundaries in Nb-doped $SrTiO_3$ bicrystals, J. Mater. Sci. **41**, 2621 (2006).

[46] S. Y. Choi, S. D. Kim, M. Choi, H. S. Lee, J. Ryu, N. Shibata, T. Mizoguchi, E. Tochigi, T. Yamamoto, S. J. L. Kang, and Y. Ikuhara, Assessment of strain-generated oxygen vacancies using $SrTiO_3$ bicrystals, Nano Lett. **15**, 4129 (2015).

[47] See Supplemental Material at http://link.aps.org/supplemental/10.1103/PhysRevB.103.L060101 for first-principles calculations, formation energy, definition of local polarization, and supporting figures and tables.

[48] C. L. Jia, L. Houben, and K. Urban, Atom vacancies at a screw dislocation core in $SrTiO_3$, Philos. Mag. Lett. **86**, 683 (2006).

[49] Z. Zhang, W. Sigle, and W. Kurtz, HRTEM and EELS study of screw dislocation cores in $SrTiO_3$, Phys. Rev. B **69**, 144103 (2004).

[50] M. Kamruzzaman, M. A. Helal, I. E. Ara, A. K. M. Farid Ul Islam, and M. M. Rahaman, A comparative study based on the first principles calculations of $ATiO_3$ (A = Ba, Ca, Pb and Sr) perovskite structure, Indian J. Phys. **90**, 1105 (2016).

[51] J. H. Haeni, P. Irvin, W. Chang, R. Uecker, P. Reiche, Y. L. Li, S. Choudhury, W. Tian, M. E. Hawley, B. Craigo *et al.*, Room-temperature ferroelectricity in strained $SrTiO_3$, Nature (London) **430**, 758 (2004).

[52] G. Sheng, Y. L. Li, J. X. Zhang, S. Choudhury, Q. X. Jia, V. Gopalan, D. G. Schlom, Z. K. Liu, and L. Q. Chen, Phase transitions and domain stabilities in biaxially strained (001) $SrTiO_3$ epitaxial thin films, J. Appl. Phys. **108**, 084113 (2010).

[53] Y. L. Li, S. Choudhury, J. H. Haeni, M. D. Biegalski, A. Vasudevarao, A. Sharan, H. Z. Ma, J. Levy, V. Gopalan, S. Trolier-McKinstry *et al.*, Phase transitions and domain structures in strained pseudocubic (100) $SrTiO_3$ thin films, Phys. Rev. B **73**, 184112 (2006).

[54] H. Uwe and T. Sakudo, Stress-induced ferroelectricity and soft phonon modes in $SrTiO_3$, Phys. Rev. B **13**, 271 (1976).

[55] R. V. K. Mangalam, N. Ray, U. V. Waghmare, A. Sundaresan, and C. N. R. Rao, Multiferroic properties of nanocrystalline $BaTiO_3$, Solid State Commun. **149**, 1 (2009).